



Novel insights on causes of disproportionate trends between particulate NO_3^- and NO_x emissions in Canadian urban atmospheres

Qinchu Fan¹, Xiaohong Yao¹, and Leiming Zhang²

¹Key Laboratory of Marine Environment and Ecology (MOE), and Frontiers Science Center for Deep Ocean Multispheres and Earth System, Sanya Oceanographic Institution, Ocean University of China, Qingdao 266100, China

²Air Quality Research Division, Science and Technology Branch, Environment and Climate Change Canada, Toronto, M3H 5T4, Canada

Correspondence: Xiaohong Yao (xhyao@ouc.edu.cn) and Leiming Zhang (leiming.zhang@ec.gc.ca)

1 **Abstract.** Particulate nitrate (NO_3^-) is a key target for controlling air pollution, yet its
2 response to NO_x abatement remains uncertain in cold climates. This study assesses
3 trends of fine- and coarse-mode NO_3^- (f- NO_3^- and c- NO_3^-) during 1990–2019 in seven
4 Canadian cities, making use of the long-term data collected by the National Air
5 Pollution Surveillance (NAPS) network, and revealed disproportionate trends between
6 NO_3^- and NO_x emissions across Canada. In Edmonton, annual mean f- NO_3^- decreased
7 by ~60% from 2007–2019 while provincial NO_x emissions declined by only 10–20%;
8 comparable patterns were also observed in five out of the six other cities in the most
9 recent decade. Such disproportionate trends were diagnosed to be caused by reduced
10 primary f- NO_3^- emissions, localized dispersion, and Arctic Oscillation–modulated wind
11 anomalies. Conversely, all cities exhibited a transient f- NO_3^- increase during 1998–
12 2007, coincident with early NO_x controls and consistent with unintended enhancement
13 of primary emissions of f- NO_3^- formed within stationary-combustion plumes. c- NO_3^-
14 was largely insensitive to NO_x reduction in most cities (except Edmonton), with its
15 trends governed by neutralization reactions with alkaline aerosols rather than HNO_3
16 availability. These findings can help interpret the weak or absent f- NO_3^- response to
17 NO_x reductions worldwide, especially in cold-climate regions.

18 **Keywords:** particulate nitrate, primary nitrate emission, decadal trends, NO_x emission
19 reduction



20 **1 Introduction**

21 Particulate nitrate (NO_3^-) has been a central focus of pollution control strategies in the
22 past several decades due to its impact on air quality, climate, and ecosystem health
23 (Balamurugan et al., 2022; Dang et al., 2024; Thunis et al., 2021; Zhai et al., 2021; Bell
24 et al., 2007; Chan et al., 2021; Cheng et al., 2024; Dabek-Zlotorzynska et al., 2011;
25 Duce et al., 2008; Font et al., 2024; Harrison et al., 2022; Man et al., 2015; Pullokaran
26 et al., 2024; Squizzato et al., 2018; Sun et al., 2025; Wang et al., 2020; Zaveri et al.,
27 2021; Zhang et al., 2008; Zhou et al., 2022). NO_3^- impacts air quality because it is a
28 major chemical component of particulate matter, especially the fine ones. Besides,
29 photolysis of NO_3^- produces highly reactive oxidants, such as hydroxyl radicals, HOCl,
30 and Cl_2 , thus enhancing atmospheric oxidation capacity (Chen et al., 2025; Gen et al.,
31 2022; Peng et al., 2022). NO_3^- contributes to climatic effects directly through radiative
32 forcing and indirectly through increasing cloud condensation nuclei (Drugé et al., 2019;
33 Zaveri et al., 2021). For instance, a modeling study showed that nitrate aerosols
34 contributed significantly to shortwave radiative cooling, reaching up to -5 W m^{-2} on a
35 regional scale under clear-sky condition and -0.8 W m^{-2} on global average (Zaveri et
36 al., 2021). NH_4NO_3 formed from condensation of gaseous species of NH_3 and HNO_3
37 can rapidly grow to the sizes of cloud condensation nuclei in cold atmospheres (Höpfner
38 et al., 2019; Wang et al., 2022; Zhu et al., 2014). Additionally, NO_3^- contributes to
39 atmospheric nitrogen deposition, which has ecosystem implications (Bose et al., 2018;
40 Iizuka et al., 2025), and it can even undergo long-range transport in the atmosphere and
41 eventually deposit into oceans or remote continental regions (Jonson et al., 2022; Qi et
42 al., 2018; Iizuka et al., 2025).

43
44 Given the significant reductions of SO_2 emissions worldwide in the past four decades,
45 the impacts of NO_3^- on air quality, climate, and ecosystem health have garnered
46 increasing attention (Aas et al., 2019; Feng et al., 2020; Hand et al., 2024; Sun et al.,
47 2018; Velazquez-Garcia et al., 2023; Wang et al., 2021; Zhai et al., 2021). Unlike



48 sulfate (SO_4^{2-}), which predominantly exists in fine particulate matter ($\text{PM}_{2.5}$), NO_3^-
 49 exists in both fine- and coarse-mode particles (referred to as f- NO_3^- and c- NO_3^- ,
 50 respectively). As a semi-volatile substance, the fine and coarse fractions of NO_3^- vary
 51 with season and location (Peng et al., 2024; Yao and Zhang, 2012a, b; Zhang et al.,
 52 2008) because its volatility and partitioning with its gaseous precursors are influenced
 53 by ambient meteorological and chemical conditions, including temperature (T), relative
 54 humidity (RH), and mixing ratios of HNO_3 and NH_3 (Guo et al., 2016; Seinfeld and
 55 Pandis, 2016; Yao et al., 2003; Huo et al., 2025). This complicates the response of f-
 56 NO_3^- and c- NO_3^- to changes in NO_x emissions (Balamurugan et al., 2022; Chan et al.,
 57 2021; Thunis et al., 2021; Zhai et al., 2021; Huo et al., 2025). Additionally, reduced
 58 NO_x emissions may enhance the formation of N_2O_5 at nighttime, a product that can
 59 form f- NO_3^- through secondary aerosol formation, thus, further influencing the
 60 response of f- NO_3^- to emission reductions (Fan et al., 2020; Shah et al., 2018; Wang et
 61 al., 2023; Yan et al., 2023; Zhou et al., 2022; Ward et al., 2025). It has been reported
 62 that f- NO_3^- can be generated from condensable species in fresh stationary combustion
 63 plumes, followed by dispersion and evaporation under freezing ambient conditions
 64 (Shen et al., 2022; Xiao et al., 2025; Yang et al., 2024; USEPA, 2016), which is an
 65 issue largely overlooked in studies examining the response of NO_3^- to NO_x emission
 66 reductions, particularly in regions experiencing long cold seasons.

67

68 Canada is a nation experiencing long cold winters. Higher concentrations of f- NO_3^-
 69 were predominantly observed during cold winter seasons, except during large-scale
 70 wildfire events mostly occurring in warm seasons (Bari and Kindzierski, 2016a, b;
 71 Dabek-Zlotorzynska et al., 2011; Edgerton et al., 2020; Jeong et al., 2011; Wang et al.,
 72 2021). The contributions of primary and/or secondary sources to the elevated f- NO_3^-
 73 concentrations in Canadian cold atmospheres remain poorly understood. The primary
 74 emissions of f- NO_3^- likely have two major sources (or processes), including (i) the rapid
 75 formation of f- NO_3^- from the reaction between $\text{HNO}_{3\text{gas}}$ and $\text{NH}_{3\text{gas}}$ within the first few
 76 seconds when combustion plumes exit the stack outlet (or vehicle exhaust pipes) and
 77 cool down, and (ii) the formation of f- NO_3^- via the reaction of $2\text{NO}_2 + \text{H}_2\text{O} \rightarrow \text{HNO}_3$



78 + HNO_2 in droplets produced in fresh cooling combustion plumes, followed by $\text{NH}_{3\text{gas}}$
79 neutralization, before these droplets evaporate into ambient aerosols. Note that the fresh
80 plumes contain extremely high concentrations of various air pollutants, enabling the
81 occurrence of the above-mentioned reaction (Seinfeld and Pandis, 2016; Zhang et al.,
82 2021; Zhang et al., 2023). The knowledge gap hinders our understanding on the impact
83 of changing primary f-NO_3^- emissions on the annual-scale response of f-NO_3^- to NO_x
84 emission reductions. Additionally, significant decreases in NO_x emissions across
85 Canada mainly occurred between 1998 and 2008, with slight time shifting across
86 different provinces (ECCC, 2021). $\text{PM}_{2.5}$ speciation data since 2003 alone may not fully
87 elucidate the response of NO_3^- to reduced NO_x emissions. Fortunately, both f-NO_3^- and
88 c-NO_3^- data are available from the National Air Pollution Surveillance (NAPS) at 12
89 urban sites (Dabek-Zlotorzynska et al., 2019; Dabek-Zlotorzynska et al., 2011). Seven
90 of these 12 sites have integrated measurements of particulate chemical components
91 spanning 1-3 decades, enabling the examination of long-term trends in f-NO_3^- and c-
92 NO_3^- in Canadian urban atmospheres and their responses to reduced NO_x emissions.

93

94 In this study we investigated long-term trends in the annual average mass
95 concentrations of f-NO_3^- and c-NO_3^- in Canadian urban atmospheres, with a particular
96 focus on the responses of f-NO_3^- and c-NO_3^- to NO_x emission reductions since 1990
97 and the associated mechanisms. The analyses include three major parts, with Part 1
98 focusing on the long-term trends of f-NO_3^- and c-NO_3^- , firstly in Edmonton (Section
99 3.1) and then extended the other six cities (Sections 3.2 and 3.3), Part 2 investigating
100 key driving factors influencing f-NO_3^- levels in Edmonton (Section 3.4) and the role of
101 primary f-NO_3^- emissions on its trends (Section 3.5), and Part 3 providing a
102 comprehensive assessment of uncertainties associated with f-NO_3^- and their potential
103 impact on the observed trends (Section 3.6). Finally, a summary of the major findings
104 and potential implications are presented in Section 4.



105 **2 Methodology**

106 **2.1 Monitoring sites and data sources**

107 The present study utilized long-term data monitored at two urban sites in Edmonton (S-
108 90132, Latitude: 53.486, Longitude: -113.465; and S-90130, Latitude: 53.544,
109 Longitude: -113.499), as well as one urban site in each of the other six cities, including
110 Winnipeg (49.898, -97.147), Victoria (48.442, -123.363), Vancouver (49.281, -
111 122.849), Montreal (45.543, -75.572), Quebec City (46.821, -71.221), and Hamilton
112 (45.258, -79.862) (Figures S1 and S2). The first four cities are in western Canada with
113 Edmonton in the province of Alberta, Winnipeg in the province of Manitoba, and
114 Victoria and Vancouver in the province of British Columbia. The other three cities are
115 in eastern Canada with Montreal and Quebec City in the province of Quebec and
116 Hamilton in the province of Ontario.

117

118 In Edmonton, at the S-90132 site speciation $PM_{2.5}$ samplers have been used since 2007
119 to measure mass concentrations of $PM_{2.5}$, ionic concentrations in $PM_{2.5}$, and the levels
120 of acidic and alkaline gases, with 24-h integrated sampling occurring one in every three
121 days (Bari and Kindzierski, 2016a, b). At the S-90130 site, ionic species, including
122 NO_3^- , SO_4^{2-} , NH_4^+ , Na^+ , and various elements in both $PM_{2.5}$ and $PM_{2.5-10}$ were collected
123 using Dichotomous Air Samplers (Thermo, US), with 24-h integrated sampling
124 occurring one in every six days during 1986-2005. Since no emission data were
125 available before 1990, only the data after 1990 were included in this study. The ionic
126 data were missing in 2006 at both sites. Note that the identical Dichotomous Air
127 Samplers were also used at S-90132 for several years, collecting $PM_{2.5}$, but not ionic
128 data, for comparison purpose. In Hamilton, an identical speciation sampler has been
129 used since 2013 to measure ionic components in $PM_{2.5}$ and gases, with sampling
130 occurring one in every three days. In this city, only elements have been measured in
131 samples collected by the Dichotomous Air Sampler since then. At the other five urban
132 sites selected for this study, speciation $PM_{2.5}$ data were either unavailable (Winnipeg
133 and Quebec City) or collected one in every six days after 2005 (Victoria, Vancouver,



134 and Montreal). PM_{2.5} air samplers (Thermo, US) were used in Victoria and Winnipeg
 135 after 2012, and PM_{2.5} samplers (TISCH, US) were used in Vancouver and Montreal
 136 after 2016. Corresponding NO₃⁻ data in PM_{2.5-10} were not available at these sites since
 137 then. In this study, NO₃⁻ in PM_{2.5} collected by speciation samplers was also referred to
 138 as f-NO₃⁻. The same definition is applied to f-SO₄²⁻ and f-NH₄⁺, which were used to
 139 facilitate the analysis of f-NO₃⁻.

140

141 Hourly average mass concentrations of PM_{2.5} and mixing ratios of NO₂ were also
 142 routinely measured at each site, except that no NO₂ mixing ratios were reported at S-
 143 90132. In this case, the values from S-90130 were used in this study. For certain parts
 144 of the year at the sites in Victoria and Quebec City, NO₂ mixing ratios were also
 145 unavailable. In these cases, the mixing ratios of NO₂ measured at different sites within
 146 a 1-2 km radius in the same city were used to facilitate the analysis. All the data are
 147 publicly available through the National Air Pollution Surveillance (NAPS) program
 148 network ([https://data-donnees.ec.gc.ca/data/air/monitor/national-air-pollution-](https://data-donnees.ec.gc.ca/data/air/monitor/national-air-pollution-surveillance-naps-program/?lang=en)
 149 [surveillance-naps-program/?lang=en](https://data-donnees.ec.gc.ca/data/air/monitor/national-air-pollution-surveillance-naps-program/?lang=en)) and summarized in Table S1.

150

151 NO_x, SO₂, and NH₃ emissions data at the provincial level in Canada were obtained from
 152 [https://www.canada.ca/en/environment-climate-change/services/environmental-](https://www.canada.ca/en/environment-climate-change/services/environmental-indicators/air-pollutant-emissions.html)
 153 [indicators/air-pollutant-emissions.html](https://www.canada.ca/en/environment-climate-change/services/environmental-indicators/air-pollutant-emissions.html). The monthly average wind fields were
 154 downloaded from <https://psl.noaa.gov/data/gridded/data.narr.html> (Figures 1 and S1),
 155 and the Arctic Oscillation (AO) Indexes were obtained from
 156 <https://www.ncdc.noaa.gov/teleconnections/ao/> (Figure S1d). Ground-level
 157 meteorological data from the airports of these cities were also downloaded from
 158 <https://www.wunderground.com/about/data>.

159

160 It is noted that existing techniques measuring ambient HNO_{3gas} have certain extents of
 161 artifacts. Specifically, the Na₂CO₃-coated denuder in speciation samplers is designed
 162 to remove all acidic gases upstream of PM_{2.5} sampling on the Teflon filter and to
 163 minimize positive artifacts on the collected PM_{2.5} (Dabek-Zlotorzynska et al., 2019;



164 Dabek-Zlotorzynska et al., 2011). The measured concentrations of $\text{HNO}_{3\text{gas}}$ using the
 165 denuder technique always include $\text{HNO}_{3\text{gas}}$, $\text{N}_2\text{O}_{5\text{gas}}$, and other acidic gases that can
 166 react with Na_2CO_3 to form NaNO_3 , and thus represent the upper values of ($\text{HNO}_{3\text{gas}}$ +
 167 $\text{N}_2\text{O}_{5\text{gas}}$). Therefore, the measured value is marked as $\text{HNO}_{3\text{gas}}^*$ instead of $\text{HNO}_{3\text{gas}}$ in
 168 the discussion below to avoid misunderstanding.

169 2.2 Statistical analysis

170 Annual average mass concentrations of f-NO_3^- and c-NO_3^- were calculated from all
 171 available data in each calendar year. However, data loss was common in each city and
 172 year despite sampling occurring one in every three or six days. To minimize uncertainty
 173 from data loss and ensure sufficient data for trend analysis, data for trend analysis were
 174 excluded for any year when measurements for two consecutive months were
 175 unavailable. To analyze the time series of the annual average mass concentrations of
 176 each species, the Mann-Kendall (M-K) analysis was employed. The qualitative trend
 177 results determined by the M-K method include: (i) an increasing/decreasing trend with
 178 a P value of <0.05 , (ii) a probable increasing/decreasing trend with a P value between
 179 0.05 and 0.1 , (iii) a stable trend with a P value >0.1 , as well as a ratio of <1.0 between
 180 the standard deviation and the mean of the dataset, and (iv) a no trend with a $P > 0.1$
 181 and other conditions (Lin et al., 2022).

182
 183 To quantify the overall effect of climate anomalies on the annual average f-NO_3^-
 184 between a pair of two years, our recently developed identical-percentile regression
 185 analysis was used (Lin et al., 2022; Yao and Zhang, 2024). In this method, the data
 186 sizes of the paired two-year should be the same (e.g., with the same time resolution and
 187 filling up all the missing data). The two sets of data, originally in time series, are sorted
 188 separately from the smallest to the largest to generate two percentile-based data arrays,
 189 which were then used for regression analysis with the intercept being set to be zero.
 190 The regression analysis can also be conducted using data in any particular percentile
 191 range for exploring different research targets. If the data sizes of the paired two-year
 192 are different, the one with a larger size can be modified to match the one with a smaller



size using the method presented by Lin et al. (2022) and Yao and Zhang (2024) before applying the regression analysis described above. Moreover, a Random Forest (RF) model was employed to evaluate the relative importance of meteorological and seasonal timing variables in driving f-NO₃⁻ formation (Text S1), and the Flexible 0-D Atmospheric Model (F0AM) was applied to simulate secondary production of f-NO₃⁻ (Text S3).

3 Results and discussion

3.1 Complexity of particulate nitrate trends in urban atmosphere of Edmonton

As mentioned in Section 2.1, two sites (S-90130 and S-90132) in Edmonton were selected for investigation due to the discontinued data coverage at both sites. Annual average mass concentrations of f-NO₃⁻ at S-90130 from 1990 to 2005 and at S-90132 from 2007 to 2019 were analyzed to illustrate the complexity of particulate nitrate trends in the urban atmosphere (Figure 1a). As mentioned in section 2.1, data in 2006 were missing at both sites. For comparison, annual average mass concentrations of c-NO₃⁻ at S-90130 from 1990 to 2005 are also shown in Figure 1a and those of f-NH₄⁺ and f-SO₄²⁻ at S-90130 and S-90132 from 1990 to 2019 are shown in Figure S3. To facilitate analysis, annual average mixing ratios of NO₂ at S-90130 from 1995 to 2019 are shown in Figure 1b, and annual provincial total emissions of NO_x, SO₂, and NH₃ in Alberta are also presented (Figures 1b, S3a and S3c, respectively). Correlation analyses between f-NO₃⁻ (or c-NO₃⁻) and provincial total emissions of NO_x in 1990-2005 and between f-SO₄²⁻ and provincial total emissions of SO₂ in 1990-2019 are conducted (Figures 1c and S3b, respectively).

At S-90130, annual average f-NO₃⁻ and c-NO₃⁻ was $0.48 \pm 0.25 \mu\text{g m}^{-3}$ (average \pm standard deviation) and $0.15 \pm 0.05 \mu\text{g m}^{-3}$, respectively, during 1990 - 2005. No trend or stable trend was found for these species ($P > 0.10$), likely due to a bell-shaped change in provincial total NO_x emissions from 1990 to 2005. In fact, a significant correlation was found between annual average c-NO₃⁻ and provincial total NO_x emissions during



1990-2005 ($P < 0.01$). However, a significant correlation between annual average f- NO_3^- and provincial NO_x emissions was obtained only during 1992-2005 ($P < 0.01$), but not for the entire period during 1990-2005 with the values in 1990-1991 being substantially deviating from the regression curve. Such a deviation is yet to be explained. At S-90132, annual average f- NO_3^- was $1.3 \pm 0.40 \mu\text{g m}^{-3}$ during 2007 - 2019. f- NO_3^- exhibited a decreasing trend ($P < 0.01$), with a Sen's Slope of $0.063 \mu\text{g m}^{-3} \text{ yr}^{-1}$, resulting in an overall decrease of approximately 60% during this period. In comparison, the monitored NO_2 mixing ratios at a different site (S-90130) decreased by approximately 20%, while provincial total NO_x emissions in Alberta were reduced by only ~10% during the same period. Such disproportionate decreases were also identified for both f- NO_3^- and c- NO_3 at S-90130 in the selected period of 1997-2005, with a ~60% decrease in their annual average concentrations compared to a ~20% decrease in both the NO_2 mixing ratios and provincial NO_x total emissions. The disproportionate large decrease in the annual average f- NO_3^- at S-90132 relative to the reduction in provincial NO_x emissions is analyzed below by considering major driving factors (Section 3.4), primary and secondary sources (Section 3.5), and potential uncertainties in the data of the generated annual average f- NO_3^- (Sections 3.6). It should be noted that the annual average f- NO_3^- measured at S-90132 in 2007-2019 were significantly higher than those recorded at S-90130 in 1990-2005 ($P < 0.01$), which could be attributed to an unexpected mitigation effect, as analyzed in Section 3.3 below.

Unlike f- NO_3^- , annual average f- SO_4^{2-} exhibited a relatively smooth decreasing trend ($P < 0.01$), with a Sen's slope of $0.029 \mu\text{g m}^{-3} \text{ yr}^{-1}$ if combining data at S-90130 from 1990 to 2005 and at S-90132 from 2007 to 2019 together (Figure S3a). This trend was mostly consistent with a $0.021 \mu\text{g m}^{-3} \text{ yr}^{-1}$ decrease in the provincial total SO_2 emissions from 1990 to 2019. Additionally, a moderately strong correlation was found between the annual average f- SO_4^{2-} and the provincial total SO_2 emissions over the three decades ($P < 0.01$, Figure S3b). The f- SO_4^{2-} trend in the urban atmosphere reflects the mitigation effect, as has also been reported for rural atmospheres in Canada (Cheng and Zhang, 2017; Feng et al., 2020). f- SO_4^{2-} , typically formed through in-cloud aqueous reactions



and with non-volatile properties, is generally associated with regional sources, and thus tends to be spatially homogeneously distributed in urban scales (Bell et al., 2007; He et al., 2001; Park et al., 2004). This may explain the much smaller gaps in the annual average f-SO_4^{2-} between the two nearby urban sites, as compared to the case of f-NO_3 . Annual average f-NH_4^+ exhibited a decreasing trend ($P < 0.05$) if combining data at S-90130 from 1990 to 2005 and at S-90132 from 2007 to 2019 (Figure S3c). However, the trend was stable at both sites during the two separate periods ($P > 0.10$). From 1990 to 2019, the provincial total NH_3 emissions increased by approximately 40% (Figure S3c). The phenomenon of the decoupled trends between f-NH_4^+ and NH_3 emissions widely occurred in Canada and the U.S. in the recent decades, as reported in Yao and Zhang (2019). This is because the level of f-NH_4^+ was mainly controlled by those of SO_4^{2-} and NO_3^- through neutralization reactions, especially under NH_3 -rich conditions (Bari and Kindzierski, 2016b; Dabek-Zlotorzynska et al., 2011; Edgerton et al., 2020). The equivalent ratios of NH_4^+ to $(\text{SO}_4^{2-} + \text{NO}_3^-)$ in two selected years support this hypothesis (Figure S4).

3.2 Trends of f-NO_3^- and c-NO_3^- in urban atmospheres of Winnipeg – an inland city in western Canada

The annual average f-NO_3^- in Winnipeg varied within a range of $0.07\text{--}0.70\text{ }\mu\text{g m}^{-3}$, with a long-term average of $0.32 \pm 0.15\text{ }\mu\text{g m}^{-3}$ from 1990 to 2018. A stable trend in annual average f-NO_3^- was identified by the M-K method ($P = 0.51$; Figure 2a). The annual average c-NO_3^- varied within an even smaller range of $0.13\text{--}0.29\text{ }\mu\text{g m}^{-3}$, with a long-term average of $0.19 \pm 0.04\text{ }\mu\text{g m}^{-3}$ during 1990–2012. A probable increasing trend in annual average c-NO_3^- was identified ($P = 0.06$). Over the same period, both the annual average mixing ratio of NO_2 at this site and provincial total NO_x emissions in Manitoba exhibited decreasing trends ($P < 0.01$) (Figure 2b), and they correlated with each other strongly ($R^2 = 0.90$, $P < 0.01$). The absence of a corresponding decrease in f-NO_3^- concentration compared to NO_x emissions is likely attributable to enhanced primary emissions of f-NO_3^- -containing aerosols, as discussed in Sections 3.3 and 3.5 below.



280 This is clearly supported by the following evidence: from 1999 to 2004, annual average
 281 f-NO_3^- increased by approximately 200%, even as provincial NO_x emissions and NO_2
 282 mixing ratios declined by about 10%. Accordingly, the trend in f-NO_3^- concentrations
 283 was analyzed in two separate periods: 1990–2002 and 2003–2018. The year of 2003 is
 284 allocated into the second rather than the first period based on the curve of annual
 285 variation shown in Figure 2a. In the first period (1990–2002), f-NO_3^- showed a probable
 286 decreasing trend, with a Sen’s Slope of $0.017 \mu\text{g m}^{-3} \text{ year}^{-1}$ and a total decline of about
 287 80%. This sharp decrease cannot be explained by the relatively modest 10–20%
 288 reductions in NO_2 and NO_x during the same period, suggesting that highly localized
 289 factors and/or uncertainties caused by coarse resolution data (1 in every 6 days) were
 290 likely the dominant contributors. The related uncertainty analysis is presented in
 291 Section 3.6 below. In the second period (2003–2018), f-NO_3^- exhibited a decreasing
 292 trend with a Sen’s Slope of $0.018 \mu\text{g m}^{-3} \text{ year}^{-1}$, amounting to an overall reduction of
 293 approximately 70%, which also exceeded the ~50% reduction in NO_2 mixing ratios at
 294 the same site and the ~30% reduction in provincial NO_x emissions. The
 295 disproportionate trends between f-NO_3^- and NO_x emissions observed in Winnipeg are
 296 similar to the case in Edmonton discussed above.

297

298 When the time series of daily concentrations of f-NO_3^- and c-NO_3^- were examined for
 299 a low-concentration year (1996) and a high-concentration year (2007) (Figure 2c–f),
 300 elevated concentrations of f-NO_3^- were predominantly observed during the cold
 301 months. High concentrations of f-NO_3^- were likely from primary sources, as discussed
 302 in Section 3.5 below, considering the similar climate in inland western Canada. This,
 303 however, needs to be confirmed using $\text{HNO}_{3\text{gas}}^*$ data, which are not available at this
 304 site. In contrast, elevated concentrations of c-NO_3^- typically occurred during warmer
 305 months. Given the probable increasing trend in annual average c-NO_3^- despite
 306 decreasing NO_x emissions at both city and provincial scales, and considering the
 307 seasonal pattern of elevated levels, it is likely that the trend in c-NO_3^- was governed by
 308 the availability of alkali aerosols capable of neutralizing $\text{HNO}_{3\text{gas}}^*$, rather than by
 309 changes in $\text{HNO}_{3\text{gas}}^*$ itself. This interpretation is also supported by findings reported in



310 literature at rural sites in Canada (Cheng and Zhang, 2017; Feng et al., 2020) and urban
 311 and rural sites in the U.S. (Sickles II and Shadwick, 2015) and U.K. (Tang et al., 2018),
 312 where positive correlations between $\text{HNO}_{3\text{gas}}^*$ and NO_2 have been observed, suggesting
 313 that a reduction in NO_x would not typically lead to enhanced $\text{HNO}_{3\text{gas}}^*$ formation.

314 **3.3 Time window for unintended effects of NO_x mitigation on f- NO_3^- aerosols in** 315 **Canadian urban atmospheres and associated shaped trends of f- NO_3^- and c- NO_3^-**

316 Long-term trends of f- NO_3^- could be distorted by unintentionally increased f- NO_3^-
 317 primary emissions resulted from certain NO_x mitigation measures. Such phenomena
 318 were repeatedly observed in urban atmospheres across Canada during a consistent time
 319 window from approximately 1998 to 2007, as illustrated in Figures 3, 4, and S5 as well
 320 as those aforementioned in Edmonton and Winnipeg. During this period, similar NO_x
 321 mitigation actions were taken in both Canada and the U.S., regulated by the Canada -
 322 U.S. Air Quality Agreement signed in 1991 and further expanded in 2000. Although
 323 mitigation policies were likely implemented independently in each province in Canada,
 324 and the exact timing may have varied slightly, a consistent pattern emerged. For
 325 example, in the province of Quebec, the annual average f- NO_3^- increased by
 326 approximately 150% in Quebec City from 1998 to 2003 and by around 300% in
 327 Montreal from 1998 to 2002. During the same period, annual average mixing ratio of
 328 NO_2 decreased by approximately 10% in both cities, while provincial total NO_x
 329 emissions remained nearly unchanged. In the province of Ontario, annual average f-
 330 NO_3^- in Hamilton remained relatively low at $0.69 \pm 0.09 \mu\text{g m}^{-3}$ during 1995–1999, but
 331 rose sharply to $1.6 \mu\text{g m}^{-3}$ in 2001, with a notable dip to $0.85 \mu\text{g m}^{-3}$ in 2002 possibly
 332 due to climate anomaly, bounced back to $1.7 \mu\text{g m}^{-3}$ in 2004 and stabilized at $1.6 \mu\text{g m}^{-3}$
 333 in 2005. During the period from 1999 - 2005, both observed NO_2 mixing ratios in
 334 Hamilton and provincial NO_x emissions in Ontario began to decline by 20–30%. A
 335 similar pattern was also found in western coastal urban areas such as Victoria and
 336 Vancouver, both located in British Columbia, between 1998 and 2002 (Figure 4), where
 337 annual average f- NO_3^- increased by approximately 100% while NO_2 mixing ratios and
 338 provincial NO_x emissions declined by 10–30%. These widespread disproportionate



339 trends between $f\text{-NO}_3^-$ and NO_x emissions across multiple cities strongly suggest the
 340 existence of the unintended effect of increased $f\text{-NO}_3^-$ primary emissions from NO_x
 341 mitigation measures during this time window; however, no direct facility measurement
 342 data were made 20-year ago to verify this hypothesis. Accordingly, trend analysis of
 343 particulate nitrate should treat this period separately, with a demarcation line drawn at
 344 approximately 2002 or later.

345
 346 Setting the demarcation line at 2003 in Quebec City (noting the substantial data loss in
 347 2002 for this city) and at 2002 in Montreal, the annual average $f\text{-NO}_3^-$ decreased by
 348 more than 70% over the subsequent 16- or 17-year period, largely agree with the 40-
 349 60% reductions in NO_2 mixing ratios and provincial NO_x emissions during the same
 350 period. The slight differences in their decreasing rates could be attributed to unintended
 351 changes in primary emissions of $f\text{-NO}_3^-$ aerosols as discussed above, non-linear
 352 atmospheric chemistry process involving other chemical species, and data
 353 uncertainties, etc. Notably, the annual average $c\text{-NO}_3^-$ showed no significant trend
 354 during these periods in either city, suggesting that $c\text{-NO}_3^-$ levels may have been more
 355 strongly influenced by the presence of alkali aerosols capable of neutralizing $\text{HNO}_{3\text{gas}}^*$
 356 rather than by the availability of $\text{HNO}_{3\text{gas}}^*$ itself. Data prior to 2002 (Montreal) or 2003
 357 (Quebec City) were insufficient in duration to support robust trend analysis;
 358 nevertheless, the influence of unintended mitigation effects during this period was still
 359 evident. In comparison, if removing the demarcation line and considering the whole
 360 data record together, annual average $f\text{-NO}_3^-$ would show no clear trend from 1995 to
 361 2018 in Quebec City and a stable trend from 1997 to 2018 in Montreal. Over the full
 362 period, annual average $f\text{-NO}_3^-$ and $c\text{-NO}_3^-$ were $0.41 \pm 0.19 \mu\text{g m}^{-3}$ and $0.19 \pm 0.05 \mu\text{g}$
 363 m^{-3} , respectively, in Quebec City and $0.57 \pm 0.38 \mu\text{g m}^{-3}$ and $0.28 \pm 0.06 \mu\text{g m}^{-3}$,
 364 respectively, in Montreal.

365
 366 Similarly, if setting a demarcation line at the year of 2002 for Victoria and Vancouver,
 367 $f\text{-NO}_3^-$ would show either a significant decreasing trend or a probable decreasing trend,
 368 with a total decrease of around 40% in both cities from 2002 to 2018. These declines



369 were broadly consistent with the 30–40% decreases in both NO₂ mixing ratios and
 370 provincial NO_x emissions during the same period. From 1990 to 2002, f-NO₃⁻ showed
 371 either no trend or a stable trend, which was consistent with the trend in the provincial
 372 NO_x emissions, but inconsistent with the observed decreasing trend in NO₂ mixing ratio
 373 during this period. If looking at the full data record of c-NO₃⁻ together (from 1990 to
 374 2012 in Victoria or 2015 in Vancouver), either no trend or a stable trend was identified
 375 in either city, regardless of using the full data record or just data after the year 2002.
 376 The absence of a clear decreasing trend in c-NO₃⁻ concentration, despite significant
 377 NO_x emissions, appears to be a common feature across Canadian urban environments.
 378 Unlike the other cities aforementioned where annual average concentrations of f-NO₃⁻
 379 were much higher than those of c-NO₃⁻, in Victoria, annual average concentrations of
 380 f-NO₃⁻ and c-NO₃⁻ were similar, oscillating around $0.23 \pm 0.06 \mu\text{g m}^{-3}$ (1990 to 2018)
 381 and $0.25 \pm 0.05 \mu\text{g m}^{-3}$ (1990 to 2012), respectively. In contrast, annual average
 382 concentrations of f-NO₃⁻ ($0.16 \pm 0.05 \mu\text{g m}^{-3}$ in 1990 - 2018) were significantly smaller
 383 than that of c-NO₃⁻ ($0.31 \pm 0.05 \mu\text{g m}^{-3}$ in 1990 - 2015) ($P < 0.01$) in Vancouver, and the
 384 same conclusion can be generated if only using data in 1990-2015.

385
 386 In Hamilton, no statistically significant trends were identified for f-NO₃⁻ and c-NO₃⁻,
 387 whether considering the full time series or just the period post-2005. This is somewhat
 388 different than the cases in the other cities discussed above, suggesting potentially strong
 389 impact of local sources, besides the other main factors discussed above, considering
 390 that Hamilton is an industrial city with heavy density of industries. Annual average f-
 391 NO₃⁻ and c-NO₃⁻ in this city were $0.88 \pm 0.35 \mu\text{g m}^{-3}$ and $0.46 \pm 0.12 \mu\text{g m}^{-3}$,
 392 respectively, during the period of 1995 to 2019.

393 **3.4 Key factors influencing annual average f-NO₃⁻ and its trends in Edmonton**

394 To explore key factors influencing the annual average f-NO₃⁻ and its trends in
 395 Edmonton, we selected data from two representative years (2010 and 2015) at site S-
 396 90132 for comparative analysis. The year 2010 was chosen because in this year
 397 abnormally high annual average f-NO₃⁻ was observed compared to all the other years



398 during the period of 2007-2019, suggesting possible impact by climate anomaly in this
 399 year. The year 2015 was chosen because in this year annual average $f\text{-NO}_3^-$ represents
 400 the median value of a five-year period of 2015-2019, likely reflecting the average
 401 climatic conditions, knowing that the annual average NO_2 mixing ratio observed at a
 402 nearby site (S-90130) and the provincial total NO_x emissions were nearly constant
 403 during 2015-2019.

404

405 Through the comparative analysis, seasonal variations of $f\text{-NO}_3^-$, various single-factor
 406 effects on $f\text{-NO}_3^-$, and the impact of climate anomalies on $f\text{-NO}_3^-$ were explored. As
 407 shown in Figures 5a and 5b, higher concentrations of $f\text{-NO}_3^-$ were predominantly
 408 observed during cold months, including January to March and November to December,
 409 in both 2010 and 2015. These higher concentrations during the five cold months
 410 contributed to 81% and 88% of the annual averages in 2015 and 2010, respectively.
 411 Based on wind fields shown in Figures S1 and S2, air masses reaching to this site in the
 412 cold winter should come from the remote northern areas with low pollution levels due
 413 to the strong northwest wind, which should have lowered concentrations of $f\text{-NO}_3^-$ in
 414 the urban atmosphere. Thus, the high concentrations of $f\text{-NO}_3^-$ observed at this site
 415 should be caused by local accumulation under stagnant weather conditions. Therefore,
 416 the emissions of $f\text{-NO}_3^-$ -contained aerosols related to mitigation measures, the
 417 precursors and formation pathways of $f\text{-NO}_3^-$, and meteorological conditions during the
 418 winter period should be considered as key factors determining the annual average $f\text{-}$
 419 NO_3^- .

420

421 We then correlated the 24-hr integrated daily concentrations of $f\text{-NO}_3^-$ with ambient T,
 422 wind speed (WS), RH, and gaseous HNO_3 ($\text{HNO}_{3\text{gas}}$) to explore various single-factor
 423 effects on $f\text{-NO}_3^-$ (Figure 5). A demarcation line was observed at -3°C in 2010 and
 424 0.5°C in 2015, with substantially lower $f\text{-NO}_3^-$ concentration at T on the right than left
 425 side of the line (Figures 5a and 5e). Lower ambient T favored the gas-aerosol
 426 partitioning of NH_4NO_3 in $\text{PM}_{2.5}$ (Seinfeld and Pandis, 2016; Shah et al., 2018).
 427 However, lower ambient T also weakened photochemical reactions due to reduced



amounts of intermediate volatility organic compounds or semi-volatile organic compounds in the gas phase (McDonald et al., 2018; Wernis et al., 2022). This reduction in photochemical activity subsequently lowered the concentration of $\text{HNO}_{3\text{gas}}$ to some extent, e.g., the concentrations of $\text{HNO}_{3\text{gas}}$ observed at $T > 20^\circ\text{C}$ increased by over a factor of four relative to those at $T < -10^\circ\text{C}$ in 2015 as shown in Figures 5e. The sources of f-NO_3^- and its formation pathways during the winter period will be revisited in Section 3.5. The causes for the different T values of the demarcation line between 2010 and 2015 are not clear. The concentrations of f-NO_3^- decreased with increasing WS due to the dispersion effect, and no elevated concentrations were observed once WS is stronger than 5 m/s (Figures 5b and 5f). The concentrations of f-NO_3^- had little dependence on ambient RH (Figure 5c and 5g), e.g., the highest concentrations in both years occurred at RH of 70–80% instead of $>80\%$. The lowest concentrations of f-NO_3^- appearing at $\text{RH} < 60\%$ is because $\text{RH} < 60\%$ typically occurred at ambient T greater than 0°C in Edmonton. In addition, the relative importance of 15 major variables on f-NO_3^- concentration was examined using a Random Forest model, as detailed in Text S1. The ambient T ranked as the dominant factor, followed by $\text{PM}_{2.5}$ mass concentration, NO_2 mixing ratio, boundary layer height, etc.

It should be noted that gas–particle equilibrium between $\text{HNO}_3\text{--NH}_3$ and submicron NH_4NO_3 is unlikely to be achieved at temperatures below -10°C , given the relatively long equilibration timescales. Based on the results of characteristic timescales analysed by Wexler and Seinfeld (1990, 1992) and dynamically simulated by Meng and Seinfeld (1996), particles with diameters of approximately $0.5\text{--}0.7\ \mu\text{m}$ generally require hours to approach equilibrium – typically on the order of $\sim 1\text{--}6\ \text{h}$ with a more conservative upper bound of $\sim 6\text{--}20$. Under such low-temperature conditions, the assumption of instantaneous thermodynamic equilibrium becomes questionable; therefore, equilibrium thermodynamic modelling was not applied here. At even lower temperatures, the equilibration timescale would extend to tens of hours for highly viscous or glassy particles, as suggested by Li and Shiraiwa (2019).



458 Correlation analysis between simultaneously measured f-NO_3^- and $\text{HNO}_{3\text{gas}}^*$ showed
 459 that f-NO_3^- concentrations higher than $4 \mu\text{g m}^{-3}$ occurred when $\text{HNO}_{3\text{gas}}^*$ concentrations
 460 were lower than $0.4 \mu\text{g m}^{-3}$ in both years (Figures 5d and 5h). Thus, the high f-NO_3^-
 461 concentrations were not likely caused from the secondary formation of f-NO_3^- from
 462 $\text{HNO}_{3\text{gas}}^*$ in ambient air, as further discussed in Section 3.5 below. Considering that the
 463 concentrations of $\text{NH}_{3\text{gas}}$ (data not shown here) were generally more than one order of
 464 magnitude higher than those of $\text{HNO}_{3\text{gas}}^*$, $\text{NH}_{3\text{gas}}$ should not be the limiting factor for
 465 f-NO_3^- formation, and was therefore excluded from further analysis below.

466

467 Climate anomaly can have significant impacts on air pollution (Andersson et al., 2007;
 468 Wetherbee and Mast, 2016; Yao and Zhang, 2020). One of the factors related to climate
 469 anomaly in Canadian urban atmospheres is AO (Yao and Zhang, 2020; Burakowski et
 470 al., 2008; Higgins et al., 2002). As shown in Figures S1 and S2, the mean wind speed
 471 from January to March across Alberta decreased significantly in 2010 compared to the
 472 other years. The AO index during the winter period in 2010 was in the most negative
 473 phase observed in the last four decades (Figure S1d). Typically, the belt of strong winds
 474 circulating around 55°N latitude weakens during such a phase, which allows colder
 475 Arctic air masses to penetrate further south into the mid-latitudes (Higgins et al., 2002).
 476 The substantial decrease in WS during the winter period of 2010 likely contributed to
 477 the higher annual average f-NO_3^- in this year. It is noticed that the recorded ambient T
 478 in Edmonton in this winter was similar to the climatic mean value
 479 (<https://www.wunderground.com/about/data>), further supporting the hypothesis that it
 480 is the weakened WS caused by AO anomaly, rather than changes in T, that enhanced the
 481 accumulation of f-NO_3^- .

482

483 To further examine the effects of the AO anomaly on f-NO_3^- accumulation in 2010
 484 relative to that in 2015, we conducted the identical-percentile regression analysis
 485 between the two years (Figures 6c-e). With the intercept being forced to zero, similar
 486 to the approach commonly used in chemical experiments for establishing the standard
 487 curve (Yao et al., 2011), the slope of the regression equation was 2.74 if using all the



488 data (0th to 100th percentiles), 1.56 if using the central 50% data (25th to 75th percentiles),
 489 and 1.41 if only using the lower 50% data (0th to 50th percentiles). The differences in f-
 490 NO₃⁻ concentration between the two years were clearly enlarged when higher
 491 concentrations were included, due to the AO anomaly effect in the winter of 2010.
 492 Assuming a log-normal distribution of the data, the lower percentiles and higher
 493 percentiles data, i.e., 0th to 2.5th percentiles and 97.5th to 100th percentiles, are normally
 494 excluded from 95% confidence level. This is because these data points have lower
 495 probability densities and their corresponding values are more vulnerable to climate
 496 anomaly impact such as AO with negative and positive phases. The highest probability
 497 density should always occur at the 50th percentile, where the corresponding value
 498 should be least affected by AO. To minimize potential error from using a single value,
 499 we used the average values of the 47.5th-52.5th percentiles, which were 0.63 µg m⁻³ in
 500 2010 and 0.45 µg m⁻³ in 2015. The ratio of these two values (=1.4) was nearly identical
 501 to the slope of the regression equation using data from the 0th to 50th percentiles
 502 presented above. Thus, the annual average f-NO₃⁻ in 2010 was recalculated by the
 503 corresponding value in 2015 being multiplying by a factor of 1.4 in order to deduct the
 504 AO anomaly effect. The recalculated annual average f-NO₃⁻ in 2010 would decrease
 505 from the original value of 2.1 µg m⁻³ to 1.2 µg m⁻³. Interestingly, removing the AO
 506 effect in 2010 would only have a minor impact on the decadal trends from 2007 to 2019,
 507 e.g., the Sen's Slope only showed small changes: which was 0.063 µg m⁻³ year⁻¹ using
 508 the original annual average values including the year 2010, 0.060 µg m⁻³ year⁻¹ if
 509 excluding the year 2010, and 0.057 µg m⁻³ year⁻¹ if replacing the year 2010 value with
 510 1.2 µg m⁻³.

511
 512 Overall, the AO largely affected the annual average f-NO₃⁻ in 2010. Nevertheless, such
 513 an impact only has marginal effects on the decadal trends of f-NO₃⁻, as the AO typically
 514 oscillates between negative and positive phases within 2-3 years (Figure S1d). The
 515 enhanced or weakened effects of AO in 2-3 years can be largely canceled out in
 516 extracting the decadal trend of f-NO₃⁻. The overall effect appeared to be too small to
 517 explain the above-mentioned disproportionate responses of the annual average f-NO₃⁻



518 to the reduced NO_x emissions, and more exploration on this issue is presented in
 519 Sections 3.5 and 3.6 below.

520 **3.5 Rethinking the role of primary emissions of NH_4NO_3 during the cold season in** 521 **Canadian urban atmospheres**

522 From the analysis presented in the previous section we concluded that the high
 523 concentrations of f-NO_3^- in the winter were mainly due to local accumulation under
 524 stagnant meteorological conditions, rather than long-range transport driven by
 525 northwesterly winds. This raised the fundamental question: what is the role of primary
 526 emissions in combustion plumes or secondary formation of NH_4NO_3 in ambient air in
 527 contributing to f-NO_3^- in Canadian urban atmospheres during the cold season? To
 528 answer this question, we proposed a hypothesis, i.e., whether $\text{HNO}_{3\text{gas}}^*$ concentrations
 529 significantly increased under conditions with low f-NO_3^- concentrations compared to
 530 cases with high f-NO_3^- concentrations, and then examined the hypothesis below.
 531 Theoretical analysis and implications of the hypothesis were provided in supplementary
 532 information (Text S2).

533
 534 To examine the weaker hypothesis outlined above, we compared three groups of data,
 535 including Group 1: $T < 0^\circ\text{C}$ and $\text{f-NO}_3^- > 4 \mu\text{g m}^{-3}$, in which case there were 19 samples
 536 with average $\text{HNO}_{3\text{gas}}^*$ and f-NO_3^- concentrations being $0.15 \pm 0.09 \mu\text{g m}^{-3}$ and $8.8 \pm$
 537 $4.4 \mu\text{g m}^{-3}$, respectively; Group 2: $T < 0^\circ\text{C}$ and $\text{f-NO}_3^- < 4 \mu\text{g m}^{-3}$, in which case there
 538 were 26 samples with average $\text{HNO}_{3\text{gas}}^*$ and f-NO_3^- concentrations being 0.15 ± 0.12
 539 $\mu\text{g m}^{-3}$ and $1.3 \pm 0.7 \mu\text{g m}^{-3}$, respectively; and Group 3: $0^\circ\text{C} < T \leq 4^\circ\text{C}$, in which case
 540 there were 13 samples with average $\text{HNO}_{3\text{gas}}^*$ and f-NO_3^- concentrations being $0.15 \pm$
 541 $0.11 \mu\text{g m}^{-3}$ and $1.3 \pm 1.7 \mu\text{g m}^{-3}$, respectively. Apparently, the average $\text{HNO}_{3\text{gas}}^*$
 542 concentrations did not differ between the three Groups ($P < 0.01$); thus, the initial
 543 hypothesis has to be rejected. This suggests that the process of secondary formation of
 544 NH_4NO_3 from $\text{HNO}_{3\text{gas}}^*$ was not the main contributor to the observed high
 545 concentrations of f-NO_3^- , leaving the process of primary emissions as the only major



546 contributor. In addition, the markedly reduced f-NO_3^- concentrations at $T > 0^\circ\text{C}$ were
 547 likely due to volatilization of a portion of primarily emitted f-NO_3^- .

548

549 The above analysis results suggest that the trend of f-NO_3^- in Edmonton was likely
 550 governed by the primary emissions of f-NO_3^- aerosols, as well as the extents of their
 551 volatilization and dispersion during the cold season. The dependence of volatilization
 552 of f-NO_3^- on ambient T and dispersion on WS has been recently confirmed in
 553 observational and modeling studies (Huo et al., 2025; Peng et al., 2024; Shen et al.,
 554 2022). As mentioned in the Introduction, the primary emissions of f-NO_3^- likely have
 555 two major sources (or processes). The first source is also conventionally defined as
 556 condensable particulate emission and associated with the combustion of ($\text{N}_2 + \text{O}_2$),
 557 which produces various oxidized nitrogen species, including $\text{HNO}_{3\text{gas}}^*$, NO_x , etc.
 558 (USEPA, 2016). The amount of primary NH_4NO_3 formed from $\text{HNO}_{3\text{gas}}^*$ in cooling
 559 plumes theoretically depends on the combustion technology, the use of catalytic
 560 reduction systems employing NH_3 , and the ambient T (Zhang et al., 2021; Tayyeb Javed
 561 et al., 2007; Palash et al., 2013), which may not be controlled by NO_x emission levels.
 562 In some reported cases, mitigation measures reduced NO_x emissions, but
 563 simultaneously increased primary emissions of f-NO_3^- (Feng et al., 2020; Palash et al.,
 564 2013; Tayyeb Javed et al., 2007; Yang et al., 2024; Zhao et al., 2020). As evidences
 565 presented in Sections 3.3, this phenomenon likely occurred across various Canadian
 566 urban atmospheres. In contrast, the second source in fresh cooling plumes is directly
 567 linked to NO_x emissions through the chemical conversion of NO_2 in cooling plume
 568 droplets, although it is highly sensitive to the lifetime of these droplets (Shen et al.,
 569 2022; Wang et al., 2016; Wang et al., 2020). In addition, primary nitrate aerosols from
 570 traffic emissions were reportedly unimportant in urban atmospheres across Canada and
 571 U.S. (Jeong et al., 2020; Chalbot et al., 2013), leaving only one possibility that primary
 572 nitrate aerosols were mainly derived from stationary combustion sources.

573

574 Although secondary f-NO_3^- formation should always occur to some extent in ambient
 575 air, the relative contribution from this process to the total f-NO_3^- is very small during



the periods with high f-NO_3^- concentrations. As shown in Text S3, the modeled maximum potential contribution from secondary formation can only account for a small fraction of the observed f-NO_3^- (<15% in the baseline runs, and <45% even in the empirical-estimate runs known to have overpredictions in general). These results support the hypothesis presented above that primary f-NO_3^- was the dominant contributor to the high f-NO_3^- concentration in winter. Moreover, higher f-NO_3^- concentrations were generally observed under low wind speeds ($\text{WS} < 1\text{--}2 \text{ m s}^{-1}$). Given that the sampling site is about 17 km from the farthest urban edge, the transport time for both primary and secondary f-NO_3^- to reach the site was therefore estimated to be approximately 2–4 h. This timescale is far too short for substantial secondary formation of f-NO_3^- in such cold ambient air ($T < -10^\circ\text{C}$), unless in-source processes dominated (Shen et al., 2022; USEPA, 2016; Zhang et al., 2023). Within this 2–4 h transport window, the amount of $\text{HNO}_{3\text{gas}}^*$ dry deposition should also be minimum, especially under low-temperature conditions.

3.6 Uncertainties affecting f-NO_3^- trends in Edmonton

Three categories of uncertainties that may affect the observed trends of f-NO_3^- in Edmonton were analyzed: (i) differences in observational results between the speciation sampler and the Dichotomous sampler, (ii) spatial inhomogeneity due to highly localized factors, and (iii) artifacts introduced by the sampling frequency (e.g., every third or sixth day), which may influence the calculation of annual averages. For category (i) uncertainty, $\text{PM}_{2.5}$ mass concentrations measured by the two different instruments at site S-90132 in 2010 showed strong agreement for most samples, with occasional discrepancies at lower concentration levels (Figure S6). Specifically, when the regression intercept was forced to zero, the resulting equation was $y = 1.02 \cdot x$ ($R^2 = 0.94$), and the difference in annual average concentrations was less than 10% ($10.3 \mu\text{g m}^{-3}$ from the Dichotomous sampler vs. $11.1 \mu\text{g m}^{-3}$ from the speciation sampler).



604 For category (ii) uncertainty, Figure S7 compares real-time PM_{2.5} mass concentrations
 605 measured simultaneously at two sites 7 km apart (S-90132 and S-90130) from 2011 to
 606 2014. Other years were excluded due to significant data loss at one or both sites.
 607 Regression slopes between the two sites (with intercepts forced to zero) are 0.86, 0.82,
 608 0.58, and 0.67, with corresponding differences in annual average concentrations of
 609 21%, 15%, 40%, and 39% in 2011, 2012, 2013, and 2014, respectively. The significant
 610 year-to-year differences between the two sites are unlikely caused by mitigation
 611 policies, climate variability, or changes in the atmospheric formation pathways of
 612 PM_{2.5}, but rather by spatial inhomogeneity driven by highly localized factors that varied
 613 from year to year. The influence of such localized effects appears to be substantial and
 614 may represent an important, yet often overlooked, contributor to the disproportionately
 615 large decreases in the annual average f-NO₃⁻ relative to reductions in provincial total
 616 NO_x emissions over decadal timescales. This overlooked factor merits broader
 617 consideration in global assessments of particulate nitrate trends.

618

619 It is noted that while the annual average PM_{2.5} mass concentrations were significantly
 620 higher at S-90130 than S-90132 ($P < 0.01$) during 2010-2014, the opposite trend was
 621 observed for the annual average f-NO₃⁻, e.g., higher at S-90132 during 2007–2019
 622 compared to those at S-90130 during 1990–2005. The highest annual average f-NO₃⁻
 623 concentration at S-90130 appeared in 2000 and that at S-90132 appeared in 2010
 624 (Figure 1a). The mass fractions of f-NO₃⁻ in PM_{2.5} were 0.050 ± 0.065 in 2000 and 0.13
 625 ± 0.13 in 2010 (Figure S4), indicating that PM_{2.5} at S-90132 contained more f-NO₃⁻
 626 aerosols during 2007-2019 than at S-90130 during 1990-2005, strongly supporting the
 627 hypothesis that mitigation measures reduced NO_x emissions in Edmonton, while
 628 simultaneously increased primary f-NO₃⁻ emissions from the first source (see Section
 629 3.3) after 2005.

630

631 Concerning category (iii) uncertainty, no continuous measurements of f-NO₃⁻ were
 632 available to assess its magnitude. We thus used continuous measurements of PM_{2.5} data
 633 at S-90130 as a proxy for this evaluation. Given that the annual average PM_{2.5} mass



634 concentration in 2010 was approximately 50% larger than in 2011, the analysis was
 635 conducted using data from 2011 to 2020 instead of 2010 to 2020. Daily average $PM_{2.5}$
 636 mass concentrations were first calculated for every day of the year. Then for each year,
 637 annual average $PM_{2.5}$ mass concentrations were calculated from daily average
 638 concentrations using (i) full dataset, (ii) one in every three days data (three subsets),
 639 and (iii) one in every six days data (six subsets). Thus, a total of 10 sets of annual
 640 average $PM_{2.5}$ data series was created for the period of 2011-2020, which was then used
 641 for decadal trend analysis. The trend derived from the full dataset showed a decreasing
 642 trend with a Sen's Slope of $0.43 \mu g m^{-3} year^{-1}$. Consistent decreasing trends were also
 643 obtained from using the one in every three days subset data series, with Sen's Slope
 644 values of 0.46, 0.46, and $0.42 \mu g m^{-3} year^{-1}$, respectively, indicating an error of less than
 645 8%. When using the one in every six days subset data series, five out of six data subsets
 646 also showed a decreasing trend, with Sen's Slope values of 0.47, 0.50, 0.45, 0.45, and
 647 $0.44 \mu g m^{-3} year^{-1}$, respectively, indicating an error of less than 10% in most cases.
 648 However, one subset data series showed a probable decreasing trend, with a Sen's Slope
 649 of $0.38 \mu g m^{-3} year^{-1}$.

650
 651 Using the same approach described above, we also compared the decadal trends
 652 obtained from using one in every three days data, which are readily available, with those
 653 from using one in every six days data, which are arbitrarily split from the former data
 654 set into two subsets. One of the two subsets for $f-NO_3^-$ showed a decreasing trend with
 655 a Sen's Slope of $0.055 \mu g m^{-3} year^{-1}$, which is close to the original value of $0.063 \mu g m^{-3} year^{-1}$;
 656 however, the other subset exhibited a stable trend. For $f-SO_4^{2-}$, both subsets
 657 showed decreasing trends, with Sen's Slope values of 0.033 and $0.018 \mu g m^{-3} year^{-1}$,
 658 respectively, although deviating to some extent from the original estimate of $0.022 \mu g m^{-3} year^{-1}$.
 659 For $f-NH_4^+$, both subsets showed stable trends, consistent with the results
 660 derived from the original dataset. Overall, using one in every three or six days data can
 661 generate decadal trends with reasonable accuracy, although the obtained trends need to
 662 be interpreted carefully when the trends are not significant or the changing rates are
 663 very small.



664 4 Conclusions

665 In-depth analysis results presented in this study demonstrate that the dynamics of
666 particulate nitrate in Canadian urban atmospheres is shaped by complex interactions
667 between emission reductions, primary sources, and cold-climate meteorology. Three
668 key insights emerge:

669

670 (i) Non-linear responses of $f\text{-NO}_3^-$ to NO_x emission reductions in all the cities: Early
671 phase implementation of NO_x control measures paradoxically increased $f\text{-NO}_3^-$ during
672 1998–2007, likely due to altered combustion plume chemistry favoring rapid $f\text{-NO}_3^-$
673 formation in cold-climate conditions. Significant declines in $f\text{-NO}_3^-$ (e.g., 60% in
674 Edmonton) outpaced NO_x reductions in the most recent decade, driven by diminishing
675 primary emissions, highly localized factors, and AO induced dispersion effects.

676

677 (ii) Decoupled $c\text{-NO}_3^-$ and NO_x reductions in all the cities except Edmonton: $c\text{-NO}_3^-$
678 remained stable or increased slightly while NO_x emissions were reduced. $c\text{-NO}_3^-$ trends
679 were likely controlled by the abundance of alkali aerosols, highlighting the limited
680 efficacy of NO_x -focused policies for controlling $c\text{-NO}_3^-$.

681

682 (iii) Critical role of primary $f\text{-NO}_3^-$ emissions in winter in all the cities: Over 80% of
683 the annual $f\text{-NO}_3^-$ burden was originated from cold-season primary emissions, with
684 minimal contribution from secondary formation process, emphasizing the need for
685 season-specific mitigation strategies.

686

687 These findings necessitate a paradigm shift in air quality management, advocating for
688 strategies that explicitly address primary sources of particulate nitrate, its partitioning
689 dynamics in cold-climate condition, and alkali aerosol interactions. Future policies
690 should enhance real-time observations on chemical components in $\text{PM}_{2.5}$ to capture
691 their localized and seasonal variability and related sources, particularly in regions with
692 prolonged winter conditions.



693
 694 **Acknowledgement.** QF and XY are supported by the Natural Science Foundation of
 695 China (grant no. 41776086). We greatly appreciate all the personnel of the NAPS
 696 Partners who operate the sites across Canada and collect the field samples, and the
 697 staff of the Analysis and Air Quality section in Ottawa for the laboratory chemical
 698 analyses and QA/QC of the data used in the present study. NPRI/APEI groups are
 699 also acknowledged for their efforts in generating emissions data across Canada.

700 *Data availability.* The access of the data used in this study is described in Section 2
 701 above.

702 *Author contributions.* QF, XY and LZ designed the research, conducted the data
 703 analysis and wrote the manuscript.

704 *Competing interests.* One of the coauthors is a member of the editorial board of ACP.

705

706 **References**

- 707 Aas, W., Mortier, A., and Bowersox, V. et al.: Global and regional trends of atmospheric sulfur, Sci. Rep.,
 708 9, 953, 10.1038/s41598-018-37304-0, 2019.
- 709 Andersson, C., Langner, J., and Bergström, R.: Interannual variation and trends in air pollution over
 710 Europe due to climate variability during 1958–2001 simulated with a regional CTM coupled to the
 711 ERA40 reanalysis, Tellus Ser. B-Chem. Phys. Meteorol., 59, 77-98, 10.1111/j.1600-
 712 0889.2006.00196.x, 2007.
- 713 Balamurugan, V., Chen, J., and Qu, Z. et al.: Secondary PM_{2.5} decreases significantly less than NO₂
 714 emission reductions during COVID lockdown in Germany, Atmos. Chem. Phys., 22, 7105-7129,
 715 10.5194/acp-22-7105-2022, 2022.
- 716 Bari, M. A., and Kindzierski, W. B.: Fine particulate matter (PM_{2.5}) in Edmonton, Canada: source
 717 apportionment and potential risk for human health, Environ. Pollut., 218, 219-229,
 718 10.1016/j.envpol.2016.06.014, 2016a.
- 719 Bari, M. A., and Kindzierski, W. B.: Eight-year (2007–2014) trends in ambient fine particulate matter
 720 (PM_{2.5}) and its chemical components in the capital region of Alberta, Canada, Environ. Int., 91, 122-
 721 132, 10.1016/j.envint.2016.02.033, 2016b.
- 722 Bell, M. L., Dominici, F., and Ebisu, K. et al.: Spatial and temporal variation in PM_{2.5} chemical
 723 composition in the United States for health effects studies, Environ. Health. Perspect., 115, 989-995,
 724 10.1289/ehp.9621, 2007.
- 725 Bose, S., Rosa, M. J., and Mathilda Chiu, Y. et al.: Prenatal nitrate air pollution exposure and reduced
 726 child lung function: timing and fetal sex effects, Environ. Res., 167, 591-597,
 727 https://doi.org/10.1016/j.envres.2018.08.019, 2018.
- 728 Burakowski, E. A., Wake, C. P., Braswell, B., and Brown, D. P.: Trends in wintertime climate in the
 729 Northeastern United States: 1965–2005, J. Geophys. Res. Atmos., 113, D20114,



- 10.1029/2008JD009870, 2008.
- Chalbot, M. C., McElroy, B., and Kavouras, I. G.: Sources, trends and regional impacts of fine particulate matter in Southern Mississippi Valley: significance of emissions from sources in the Gulf of Mexico coast, *Atmos. Chem. Phys.*, 13, 3721–3732, 10.5194/acp-13-3721-2013, 2013.
- Chan, Y., Evans, M. J., and He, P. et al.: Heterogeneous nitrate production mechanisms in intense haze events in the North China Plain, *J. Geophys. Res.-Atmos.*, 126, e2021JD034688, 10.1029/2021JD034688, 2021.
- Chen, G., Fan, X., and Yu, S. et al.: HOCl formation driven by photochemical processes enhanced atmospheric oxidation capacity in a coastal atmosphere, *Environ. Sci. Technol.*, 59, 5164–5171, 10.1021/acs.est.5c01363, 2025.
- Cheng, B., Alapaty, K., and Arunachalam, S.: Spatiotemporal trends in PM_{2.5} chemical composition in the conterminous U.S. During 2006–2020, *Atmos. Environ.*, 316, 120188, 10.1016/j.atmosenv.2023.120188, 2024.
- Cheng, I., and Zhang, L.: Long-term air concentrations, wet deposition, and scavenging ratios of inorganic ions, HNO₃, and SO₂ and assessment of aerosol and precipitation acidity at Canadian rural locations, *Atmos. Chem. Phys.*, 17, 4711–4730, 10.5194/acp-17-4711-2017, 2017.
- Dabek-Zlotorzynska, E., Celo, V., and Ding, L. et al.: Characteristics and sources of PM_{2.5} and reactive gases near roadways in two metropolitan areas in Canada, *Atmos. Environ.*, 218, 116980, 10.1016/j.atmosenv.2019.116980, 2019.
- Dabek-Zlotorzynska, E., Dann, T. F., and Kalyani Martinelango, P. et al.: Canadian national air pollution surveillance (NAPS) PM_{2.5} speciation program: methodology and PM_{2.5} chemical composition for the years 2003–2008, *Atmos. Environ.*, 45, 673–686, 10.1016/j.atmosenv.2010.10.024, 2011.
- Dang, R., Jacob, D. J., and Zhai, S. et al.: A satellite-based indicator for diagnosing particulate nitrate sensitivity to precursor emissions: application to East Asia, Europe, and North America, *Environ. Sci. Technol.*, 58, 20101–20113, 10.1021/acs.est.4c08082, 2024.
- Drugé, T., Nabat, P., Mallet, M., and Somot, S.: Model simulation of ammonium and nitrate aerosols distribution in the euro-mediterranean region and their radiative and climatic effects over 1979–2016, *Atmos. Chem. Phys.*, 19, 3707–3731, 10.5194/acp-19-3707-2019, 2019.
- Duce, R. A., LaRoche, J., and Altieri, K. et al.: Impacts of atmospheric anthropogenic nitrogen on the open ocean, *Science*, 320, 893–897, 10.1126/science.1150369, 2008.
- ECCC: Environment and climate change Canada: Canadian environmental sustainability indicators: air pollutant emissions, available at: <https://www.canada.ca/en/environment-climate-change/services/environmental-indicators/air-pollutant-emissions.html>, last access: 13 November 2021., in, edited, 2021.
- Edgerton, E. S., Hsu, Y., and White, E. M. et al.: Ambient concentrations and total deposition of inorganic sulfur, inorganic nitrogen and base cations in the Athabasca oil sands region, *Sci. Total Environ.*, 706, 134864, 10.1016/j.scitotenv.2019.134864, 2020.
- Fan, M., Zhang, Y., and Lin, Y. et al.: Changes of emission sources to nitrate aerosols in Beijing after the clean air actions: evidence from dual isotope compositions, *J. Geophys. Res.-Atmos.*, 125, e2019JD031998, 10.1029/2019JD031998, 2020.
- Feng, J., Chan, E., and Vet, R.: Air quality in the Eastern United States and Eastern Canada for 1990–2015: 25 years of change in response to emission reductions of SO₂ and NO_x in the region, *Atmos. Chem. Phys.*, 20, 3107–3134, 10.5194/acp-20-3107-2020, 2020.
- Font, A., de Brito, J. F., and Riffault, V. et al.: Long-term measurements of aerosol composition at rural



- background sites in France: sources, seasonality and mass closure of PM_{2.5}, *Atmos. Environ.*, 334, 120724, 10.1016/j.atmosenv.2024.120724, 2024.
- Gen, M., Liang, Z., and Zhang, R. et al.: Particulate nitrate photolysis in the atmosphere, *Environmental Science: Atmospheres*, 2, 111-127, 10.1039/d1ea00087j, 2022.
- Guo, T., Li, K., and Zhu, Y. et al.: Concentration and size distribution of particulate oxalate in marine and coastal atmospheres – implication for the increased importance of oxalate in nanometer atmospheric particles, *Atmos. Environ.*, 142, 19-31, 10.1016/j.atmosenv.2016.07.026, 2016.
- Hand, J. L., Prenni, A. J., and Schichtel, B. A.: Trends in seasonal mean speciated aerosol composition in remote areas of the United States from 2000 through 2021, *J. Geophys. Res.-Atmos.*, 129, e2023JD039902, 10.1029/2023JD039902, 2024.
- Harrison, R. M., Beddows, D. C. S., Tong, C., and Damayanti, S.: Non-linearity of secondary pollutant formation estimated from emissions data and measured precursor-secondary pollutant relationships, *npj Clim. Atmos. Sci.*, 5, 71, 10.1038/s41612-022-00297-9, 2022.
- He, K., Yang, F., and Ma, Y. et al.: The characteristics of PM_{2.5} in Beijing, China, *Atmos. Environ.*, 35, 4959-4970, 10.1016/S1352-2310(01)00301-6, 2001.
- Higgins, R. W., Leetmaa, A., and Kousky, V. E.: Relationships between climate variability and winter temperature extremes in the United States, *J. Clim.*, 15, 1555-1572, 10.1175/1520-0442(2002)015<1555:RBCVAW>2.0.CO;2, 2002.
- Höpfner, M., Ungermann, J., and Borrmann, S. et al.: Ammonium nitrate particles formed in upper troposphere from ground ammonia sources during Asian monsoons, *Nat. Geosci.*, 12, 608-612, 10.1038/s41561-019-0385-8, 2019.
- Huo, H., Gao, Y., and Sun, L. et al.: Investigating dual character of atmospheric ammonia on particulate NH₄NO₃: reducing evaporation versus promoting formation, *Atmosphere*, 16, 685, 10.3390/atmos16060685, 2025.
- Iizuka, Y., Matsumoto, M., and Kawakami, K. et al.: Acidity-driven gas-particle partitioning of nitrate regulates its transport to arctic through the industrial era, *Nat. Commun.*, 16, 4272, 10.1038/s41467-025-59208-0, 2025.
- Jeong, C. H., McGuire, M. L., and Herod, D. et al.: Receptor model based identification of PM_{2.5} sources in Canadian cities, *Atmos. Pollut. Res.*, 2, 158-171, 10.5094/APR.2011.021, 2011.
- Jeong, C., Traub, A., and Huang, A. et al.: Long-term analysis of PM_{2.5} from 2004 to 2017 in Toronto: composition, sources, and oxidative potential, *Environ. Pollut.*, 263, 114652, 10.1016/j.envpol.2020.114652, 2020.
- Jonson, J. E., Fagerli, H., Scheuschner, T., and Tsyro, S.: Modelling changes in secondary inorganic aerosol formation and nitrogen deposition in Europe from 2005 to 2030, *Atmos. Chem. Phys.*, 22, 1311-1331, 10.5194/acp-22-1311-2022, 2022.
- Li, Y., and Shiraiwa, M.: Timescales of secondary organic aerosols to reach equilibrium at various temperatures and relative humidities, *Atmos. Chem. Phys.*, 19, 5959-5971, 10.5194/acp-19-5959-2019, 2019.
- Lin, Y., Zhang, L., and Fan, Q. et al.: Decoupling impacts of weather conditions on interannual variations in concentrations of criteria air pollutants in South China -- constraining analysis uncertainties by using multiple analysis tools, *Atmos. Chem. Phys.*, 22, 16073-16090, 10.5194/acp-22-16073-2022, 2022.
- Man, H., Zhu, Y., and Ji, F. et al.: Comparison of daytime and nighttime new particle growth at the HKUST supersite in Hong Kong, *Environ. Sci. Technol.*, 49, 7170-7178, 10.1021/acs.est.5b02143,



- 2015.
- McDonald, B. C., de Gouw, J. A., and Gilman, J. B. et al.: Volatile chemical products emerging as largest petrochemical source of urban organic emissions, *Science*, 359, 760-764, 10.1126/science.aag0524, 2018.
- Meng, Z., and Seinfeld, J. H.: Time scales to achieve atmospheric gas-aerosol equilibrium for volatile species, *Atmos. Environ.*, 30, 2889-2900, [https://doi.org/10.1016/1352-2310\(95\)00493-9](https://doi.org/10.1016/1352-2310(95)00493-9), 1996.
- Palash, S. M., Masjuki, H. H., and Kalam, M. A. et al.: State of the art of NO_x mitigation technologies and their effect on the performance and emission characteristics of biodiesel-fueled compression ignition engines, *Energy Conv. Manag.*, 76, 400-420, 10.1016/j.enconman.2013.07.059, 2013.
- Park, R. J., Jacob, D. J., and Field, B. D. et al.: Natural and transboundary pollution influences on sulfate-nitrate-ammonium aerosols in the United States: implications for policy, *J. Geophys. Res. Atmos.*, 109, 10.1029/2003JD004473, 2004.
- Peng, W., Zhu, B., and Kang, H. et al.: Inconsistent 3-d structures and sources of sulfate ammonium and nitrate ammonium aerosols during cold front episodes, *J. Geophys. Res.-Atmos.*, 129, e2023JD039958, 10.1029/2023JD039958, 2024.
- Peng, X., Wang, T., and Wang, W. et al.: Photodissociation of particulate nitrate as a source of daytime tropospheric Cl₂, *Nat. Commun.*, 13, 939, 10.1038/s41467-022-28383-9, 2022.
- Pullokaran, D., Bhardwaj, A., and Haswani, D. et al.: Spatio-temporal trends of the relationships between surface PM_{2.5} and its chemical constituents across three COALESCE network locations in India: a mass closure investigation, *J. Geophys. Res.-Atmos.*, 129, e2023JD039855, 10.1029/2023JD039855, 2024.
- Qi, J., Liu, X., and Yao, X. et al.: The concentration, source and deposition flux of ammonium and nitrate in atmospheric particles during dust events at a coastal site in Northern China, *Atmos. Chem. Phys.*, 18, 571-586, 10.5194/acp-18-571-2018, 2018.
- Seinfeld, J. H., and Pandis, S. N.: Atmospheric chemistry and physics: from air pollution to climate change. Third edition. Hoboken, new jersey: John Wiley & Sons, inc., in, edited, 2016.
- Shah, V., Jaeglé, L., and Thornton, J. A. et al.: Chemical feedbacks weaken the wintertime response of particulate sulfate and nitrate to emissions reductions over the eastern united states, *Proc. Natl. Acad. Sci.*, 115, 8110-8115, 10.1073/pnas.1803295115, 2018.
- Shen, Y., Meng, H., and Yao, X. et al.: Does ambient secondary conversion or the prolonged fast conversion in combustion plumes cause severe PM_{2.5} air pollution in China? *Atmosphere*, 13, 673, 10.3390/atmos13050673, 2022.
- Sickles II, J. E., and Shadwick, D. S.: Air quality and atmospheric deposition in the eastern US: 20 years of change, *Atmos. Chem. Phys.*, 15, 173-197, 10.5194/acp-15-173-2015, 2015.
- Squizzato, S., Masiol, M., Rich, D. Q., and Hopke, P. K.: PM_{2.5} and gaseous pollutants in New York state during 2005–2016: spatial variability, temporal trends, and economic influences, *Atmos. Environ.*, 183, 209-224, 10.1016/j.atmosenv.2018.03.045, 2018.
- Sun, P., Wang, J., and Liu, Y. et al.: Enhanced particulate nitrate formation in residual layer exacerbates near-surface pollution: insights from tethered airship and long-term ground measurements, *J. Geophys. Res.-Atmos.*, 130, e2024JD042672, 10.1029/2024JD042672, 2025.
- Sun, W., Shao, M., and Granier, C. et al.: Long-term trends of anthropogenic SO₂, NO, CO, and NMVOCs emissions in China, *Earth's Future*, 6, 1112-1133, 10.1029/2018EF000822, 2018.
- Tang, Y. S., Braban, C. F., and Dragosits, U. et al.: Acid gases and aerosol measurements in the UK (1999–2015): regional distributions and trends, *Atmos. Chem. Phys.*, 18, 16293-16324, 10.5194/acp-



- 18-16293-2018, 2018.
- Tayyeb Javed, M., Irfan, N., and Gibbs, B. M.: Control of combustion-generated nitrogen oxides by selective non-catalytic reduction, *J. Environ. Manage.*, 83, 251-289, 10.1016/j.jenvman.2006.03.006, 2007.
- Thunis, P., Clappier, A., and Beekmann, M. et al.: Non-linear response of PM_{2.5} to changes in NO_x and NH₃ emissions in the Po basin (Italy): consequences for air quality plans, *Atmos. Chem. Phys.*, 21, 9309-9327, 10.5194/acp-21-9309-2021, 2021.
- USEPA: CASTNET 2016 annual report, edited, 2016.
- Velazquez-Garcia, A., Crumeyrolle, S., and de Brito, J. F. et al.: Deriving composition-dependent aerosol absorption, scattering and extinction mass efficiencies from multi-annual high time resolution observations in Northern France, *Atmos. Environ.*, 298, 119613, 10.1016/j.atmosenv.2023.119613, 2023.
- Wang, G., Zhang, R., and Gomez, M. E. et al.: Persistent sulfate formation from London fog to Chinese haze, *Proc. Natl. Acad. Sci.*, 113, 13630-13635, 10.1073/pnas.1616540113, 2016.
- Wang, H., Wang, H., and Lu, X. et al.: Increased night-time oxidation over China despite widespread decrease across the globe, *Nat. Geosci.*, 16, 217-223, 10.1038/s41561-022-01122-x, 2023.
- Wang, H., Zhang, L., and Cheng, L. et al.: Spatiotemporal trends of PM_{2.5} and its major chemical components at urban sites in Canada, *J. Environ. Sci.*, 103, 1-11, 10.1016/j.jes.2020.09.035, 2021.
- Wang, M., Kong, W., and Marten, R. et al.: Rapid growth of new atmospheric particles by nitric acid and ammonia condensation, *Nature*, 581, 184-189, 10.1038/s41586-020-2270-4, 2020.
- Wang, M., Xiao, M., and Bertozzi, B. et al.: Synergistic HNO₃-H₂SO₄-NH₃ upper tropospheric particle formation, *Nature*, 605, 483-489, 10.1038/s41586-022-04605-4, 2022.
- Ward, R. X., Baliak, H. D., and Schulze, B. C. et al.: Poorly quantified trends in ammonium nitrate remain critical to understand future urban aerosol control strategies, *Sci. Adv.*, 11, eadt8957, 10.1126/sciadv.adt8957, 2025.
- Wernis, R. A., Kreisberg, N. M., and Weber, R. J. et al.: Source apportionment of VOCs, IVOCs and SVOCs by positive matrix factorization in suburban Livermore, California, *Atmos. Chem. Phys.*, 22, 14987-15019, 10.5194/acp-22-14987-2022, 2022.
- Wetherbee, G. A., and Mast, M. A.: Annual variations in wet-deposition chemistry related to changes in climate, *Clim. Dyn.*, 47, 3141-3155, 10.1007/s00382-016-3017-7, 2016.
- Wexler, A. S., and Seinfeld, J. H.: The distribution of ammonium salts among a size and composition dispersed aerosol, *Atmospheric Environment. Part A. General Topics*, 24, 1231-1246, [https://doi.org/10.1016/0960-1686\(90\)90088-5](https://doi.org/10.1016/0960-1686(90)90088-5), 1990.
- Wexler, A. S., and Seinfeld, J. H.: Analysis of aerosol ammonium nitrate: departures from equilibrium during SCAQS, *Atmospheric Environment. Part A. General Topics*, 26, 579-591, [https://doi.org/10.1016/0960-1686\(92\)90171-G](https://doi.org/10.1016/0960-1686(92)90171-G), 1992.
- Xiao, H., Chen, T., and Zhang, Q. et al.: Changes in the dominant contributions of nitrate formation and sources during haze episodes: insights from dual isotopic evidence, *J. Geophys. Res.-Atmos.*, 130, e2024JD042175, 10.1029/2024JD042175, 2025.
- Yan, C., Tham, Y. J., and Nie, W. et al.: Increasing contribution of nighttime nitrogen chemistry to wintertime haze formation in Beijing observed during COVID-19 lockdowns, *Nat. Geosci.*, 16, 975-981, 10.1038/s41561-023-01285-1, 2023.
- Yang, T., Li, H., and Xu, W. et al.: Strong impacts of regional atmospheric transport on the vertical distribution of aerosol ammonium over Beijing, *Environ. Sci. Technol. Lett.*, 11, 29-34,



- 906 10.1021/acs.estlett.3c00791, 2024.
- 907 Yao, X., Lau, A. P. S., and Fang, M. et al.: Size distributions and formation of ionic species in atmospheric
 908 particulate pollutants in Beijing, China: 1—inorganic ions, *Atmos. Environ.*, 37, 2991-3000,
 909 10.1016/S1352-2310(03)00255-3, 2003.
- 910 Yao, X., Lee, C. J., and Evans, G. J. et al.: Evaluation of ambient SO_2 measurement methods at roadside
 911 sites, *Atmos. Environ.*, 45, 2781-2788, <https://doi.org/10.1016/j.atmosenv.2011.01.070>, 2011.
- 912 Yao, X., and Zhang, L.: Chemical processes in sea-salt chloride depletion observed at a Canadian rural
 913 coastal site, *Atmos. Environ.*, 46, 189-194, 10.1016/j.atmosenv.2011.09.081, 2012a.
- 914 Yao, X., and Zhang, L.: Supermicron modes of ammonium ions related to fog in rural atmosphere, *Atmos.*
 915 *Chem. Phys.*, 12, 11165-11178, 10.5194/acp-12-11165-2012, 2012b.
- 916 Yao, X., and Zhang, L.: Causes of large increases in atmospheric ammonia in the last decade across
 917 North America, *ACS Omega*, 4, 22133-22142, 10.1021/acsomega.9b03284, 2019.
- 918 Yao, X., and Zhang, L.: Decoding long-term trends in the wet deposition of sulfate, nitrate, and
 919 ammonium after reducing the perturbation from climate anomalies, *Atmos. Chem. Phys.*, 20, 721-733,
 920 <http://doi.org/10.5194/acp-20-721-2020>, 2020.
- 921 Yao, X., and Zhang, L.: Identifying decadal trends in deweathered concentrations of criteria air pollutants
 922 in Canadian urban atmospheres with machine learning approaches, *Atmos. Chem. Phys.*, 24, 7773-
 923 7791, 10.5194/acp-24-7773-2024, 2024.
- 924 Zaveri, R. A., Easter, R. C., and Singh, B. et al.: Development and evaluation of chemistry-aerosol-
 925 climate model CAM5-chem-MAM7-MOSAIC: global atmospheric distribution and radiative effects
 926 of nitrate aerosol, *J. Adv. Model. Earth Syst.*, 13, e2020MS002346, 10.1029/2020MS002346, 2021.
- 927 Zhai, S., Jacob, D. J., and Wang, X. et al.: Control of particulate nitrate air pollution in China, *Nat. Geosci.*,
 928 14, 389-395, 10.1038/s41561-021-00726-z, 2021.
- 929 Zhang, L., Vet, R., and Wiebe, A. et al.: Characterization of the size-segregated water-soluble inorganic
 930 ions at eight Canadian rural sites, *Atmos. Chem. Phys.*, 8, 7133-7151, 10.5194/acp-8-7133-2008, 2008.
- 931 Zhang, Q., Wang, Y., and Liu, M. et al.: Wintertime formation of large sulfate particles in China and
 932 implications for human health, *Environ. Sci. Technol.*, 57, 20010-20023, 10.1021/acs.est.3c05645,
 933 2023.
- 934 Zhang, Z., Li, Y., and Zhang, X. et al.: Review of hazardous materials in condensable particulate matter,
 935 *Fuel Process. Technol.*, 220, 106892, <https://doi.org/10.1016/j.fuproc.2021.106892>, 2021.
- 936 Zhao, S., Hu, B., and Gao, W. et al.: Effect of the “coal to gas” project on atmospheric NO_x during the
 937 heating period at a suburban site between Beijing and Tianjin, *Atmos. Res.*, 241, 104977,
 938 10.1016/j.atmosres.2020.104977, 2020.
- 939 Zhou, M., Nie, W., and Qiao, L. et al.: Elevated formation of particulate nitrate from N_2O_5 hydrolysis in
 940 the Yangtze River Delta region from 2011 to 2019, *Geophys. Res. Lett.*, 49, e2021GL097393,
 941 10.1029/2021GL097393, 2022.
- 942 Zhu, Y., Sabaliauskas, K., and Liu, X. et al.: Comparative analysis of new particle formation events in
 943 less and severely polluted urban atmosphere, *Atmos. Environ.*, 98, 655-664,
 944 10.1016/j.atmosenv.2014.09.043, 2014.

945
 946
 947 **List of Figures**



948 **Figure 1.** (a) Annual variations of mass concentrations of f-NO_3^- and c-NO_3^- in Edmonton, (b) annual
 949 variations of mixing ratio of NO_2 in Edmonton and provincial total NO_x emissions, and (c) f-NO_3^- and
 950 c-NO_3^- at S-90130 vs. NO_x emissions. Blue and black markers in (a) represent data obtained at S-90130
 951 and S-90132, respectively.

952 **Figure 2.** (a) Annual variations of mass concentrations of f-NO_3^- and c-NO_3^- in Winnipeg, (b) annual
 953 variations of mixing ratio of NO_2 in Winnipeg and provincial total NO_x emissions, and time series of 24-
 954 h integrated sample at a time resolution of one in every three days: (c) f-NO_3^- in 1996, (d) c-NO_3^- in
 955 1996, (e) f-NO_3^- in 2007, and (f) c-NO_3^- in 2007. Blue and black markers in (a) represent data points
 956 before and after 2003, respectively.

957 **Figure 3.** (a) Annual variations of mass concentrations of f-NO_3^- and c-NO_3^- in Quebec City, (b) annual
 958 variations of mixing ratio of NO_2 in Quebec City and provincial total NO_x emissions, (c) f-NO_3^- and c-
 959 NO_3^- in Montreal, and (d) NO_2 mixing ratio in Montreal. Blue and black markers in (a) and (c) represent
 960 data points before and after 2003 (2002), respectively.

961 **Figure 4.** Same as in Figure 3 except for Victoria (a and b) and Vancouver (c and d). Blue and black
 962 markers in (a) and (c) represent data points before and after 2002, respectively.

963 **Figure 5.** Single-factor (T, WS, RH, and $\text{HNO}_{3\text{gas}}^*$) effects on daily f-NO_3^- (and HNO_3^* in the case of T
 964 factor) in 2010 and 2015.

965 **Figure 6.** Time series of 24-h integrated f-NO_3^- in 2010 (a) and 2015 (b) in Edmonton at a time resolution
 966 of one sample in every three days, and correlations in the re-constructed f-NO_3^- between 2015 and 2010
 967 using data points with values of full range (0^{th} - 100^{th} percentiles) (c), central 50% (25^{th} - 75^{th} percentile)
 968 (d), and lower 50% (0^{th} - 50^{th} percentile) (e).

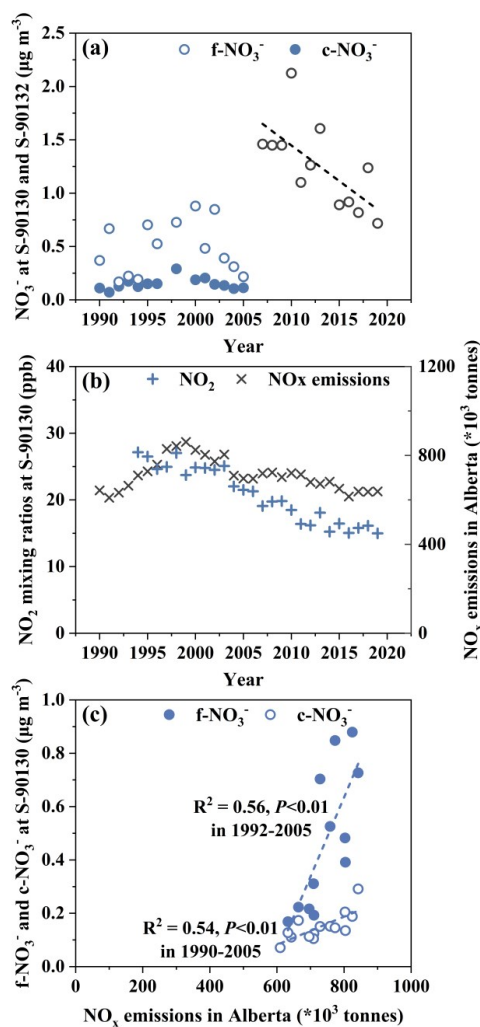


Figure 1. (a) Annual variations of mass concentrations of f-NO₃⁻ and c-NO₃⁻ in Edmonton, (b) annual variations of mixing ratio of NO₂ in Edmonton and provincial total NO_x emissions, and (c) f-NO₃⁻ and c-NO₃⁻ at S-90130 vs. NO_x emissions. Blue and black markers in (a) represent data obtained at S-90130 and S-90132, respectively.

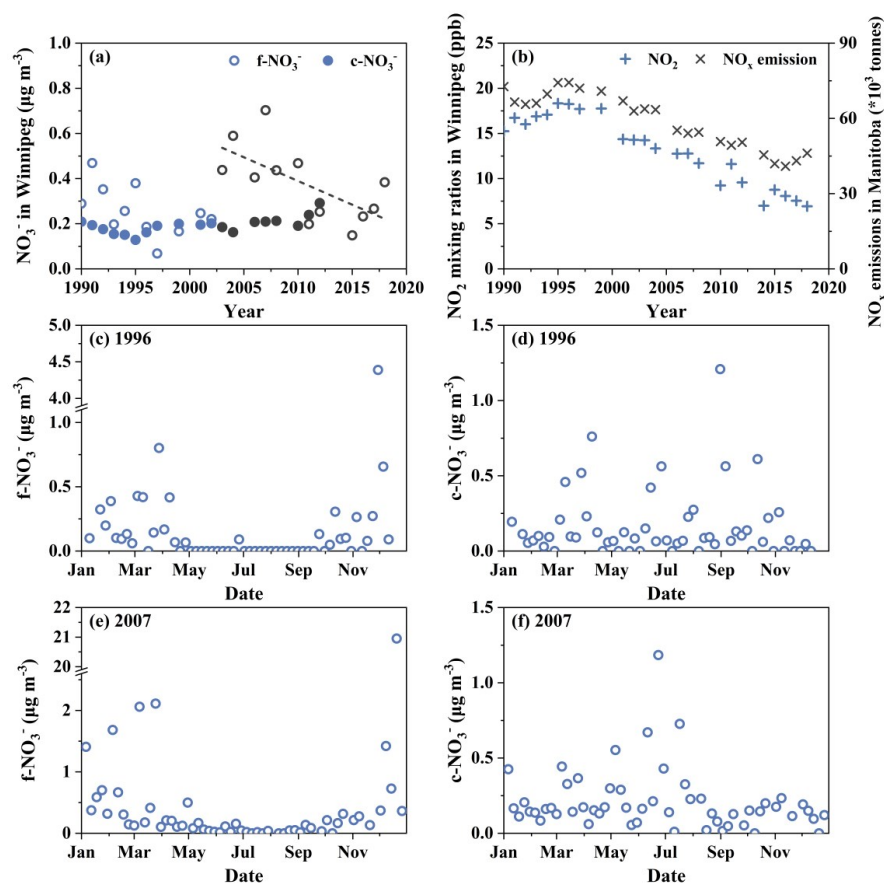


Figure 2. (a) Annual variations of mass concentrations of f-NO₃⁻ and c-NO₃⁻ in Winnipeg, (b) annual variations of mixing ratio of NO₂ in Winnipeg and provincial total NO_x emissions, and time series of 24-h integrated (c) f-NO₃⁻ in 1996, (d) c-NO₃⁻ in 1996, (e) f-NO₃⁻ in 2007, and (f) c-NO₃⁻ in 2007, at a time resolution of one sample in every three days. Blue and black markers in (a) represent data points before and after 2003, respectively.

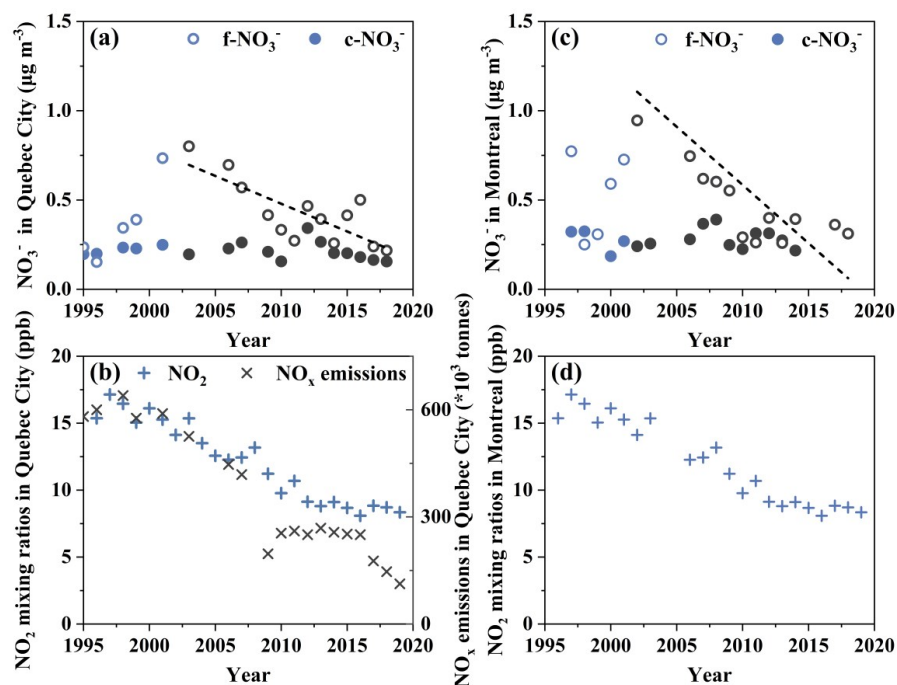


Figure 3. (a) Annual variations of mass concentrations of f-NO_3^- and c-NO_3^- in Quebec City, (b) annual variations of mixing ratio of NO_2 in Quebec City and provincial total NO_x emissions, (c) f-NO_3^- and c-NO_3^- in Montreal, and (d) NO_2 mixing ratio in Montreal. Blue and black markers in (a) and (c) represent data points before and after 2003 (2002), respectively.

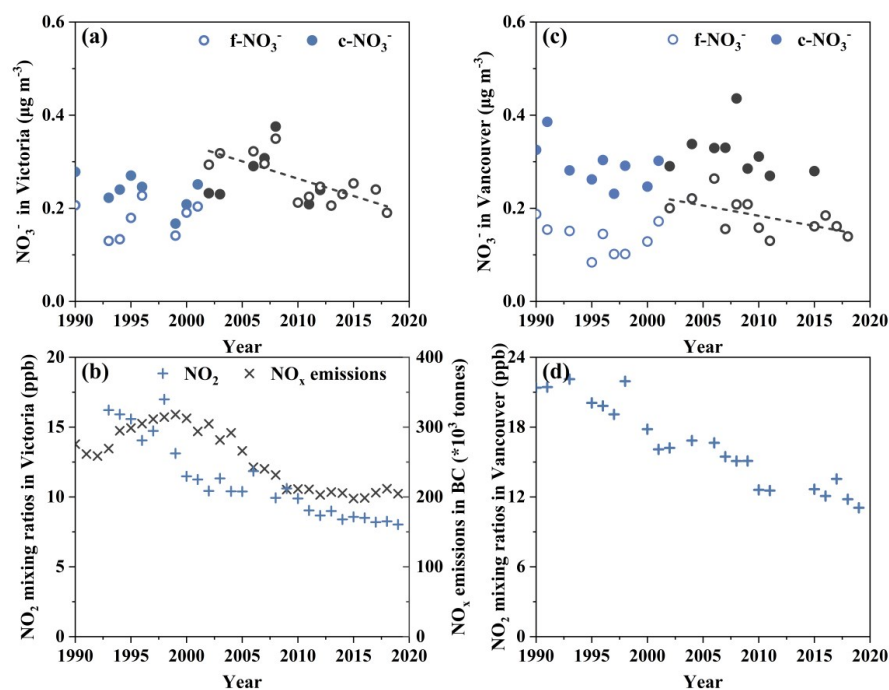


Figure 4. Same as in Figure 3 except for Victoria (a and b) and Vancouver (c and d).

Blue and black markers in (a) and (c) represent data points before and after 2002, respectively.

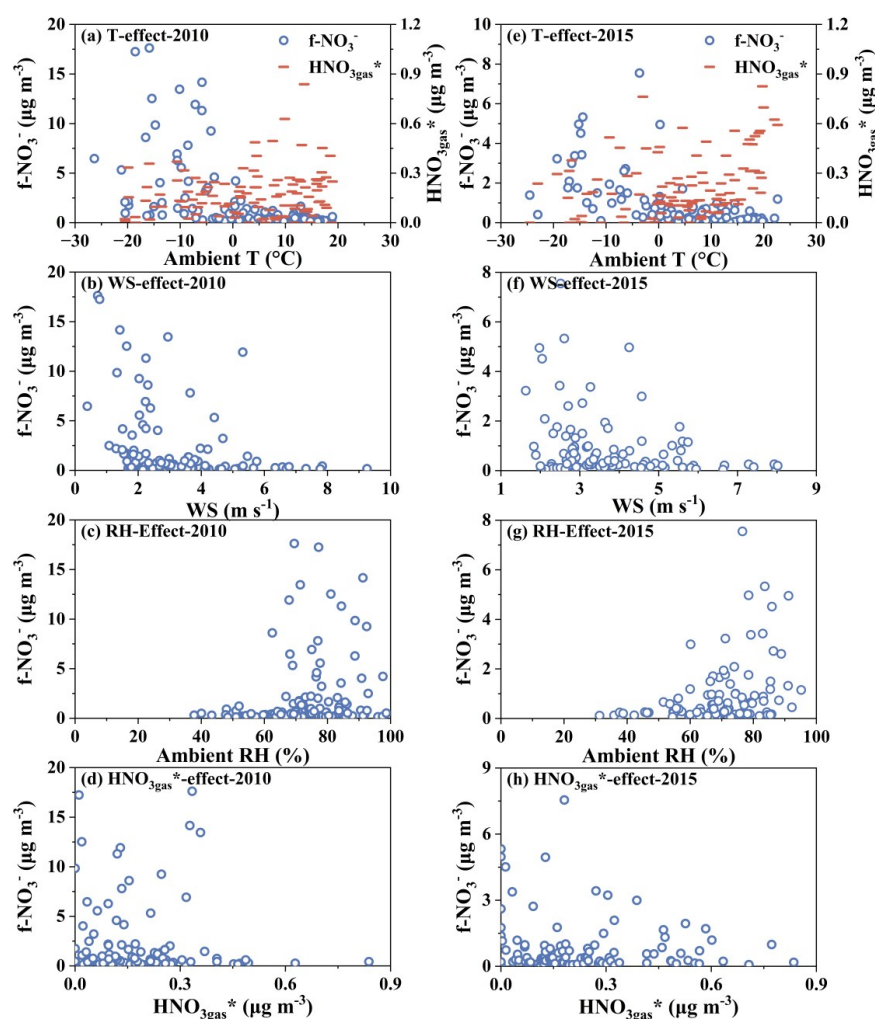


Figure 5. Single-factor (T, WS, RH, and $\text{HNO}_{3\text{gas}}^*$) effects on daily $f\text{-NO}_3^-$ (and HNO_3^* in the case of T factor) in 2010 and 2015.

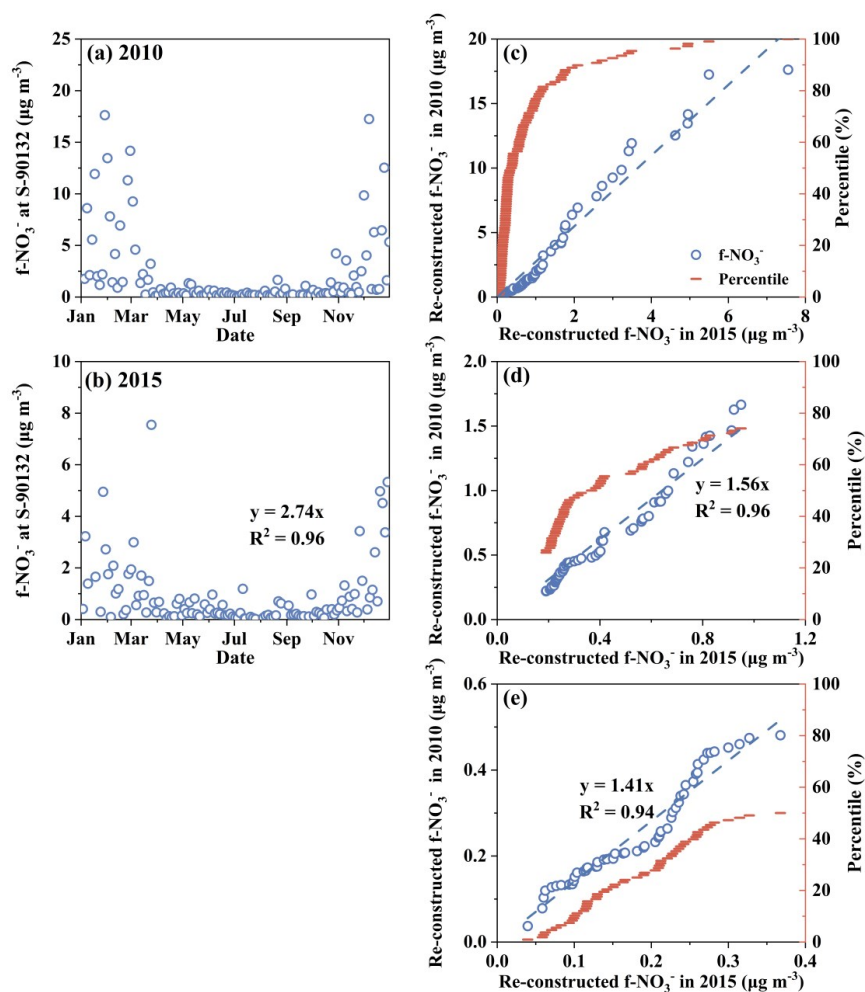


Figure 6. Time series of 24-h integrated $f\text{-NO}_3^-$ in 2010 (a) and 2015 (b) in Edmonton at a time resolution of one sample in every three days, and correlations in the re-constructed $f\text{-NO}_3^-$ between 2015 and 2010 using data points with values of full range (0th-100th percentiles) (c), central 50% (25th-75th percentile) (d), and lower 50% (0th-50th percentile) (e).